A Novel C-Terminal Mutation in *Gsdma3* (C+/H−) Leads to Alopecia and Corneal Inflammatory Response in Mice

Sebastian Swirski,[1] Carsten Röger,*,[1] Aldona Pieńkowska-Schelling,[2] Cynthia Ihlenburg,[3] Gösta Fischer,[3] Oliver May,[1] Mariann Vorm,[1] Marta Owczarek-Lipska,[1] and John Neidhardt[1,4]

[1]Human Genetics, Faculty of Medicine and Health Sciences, University of Oldenburg, Oldenburg, Germany
[2]Institute of Genetics, University of Bern, Bern, Switzerland
[3]Institut für Pathologie Prof. Dr. G. Fischer & Partner, Wilhelmshaven, Germany
[4]Research Center Neurosensory Science, University Oldenburg, Oldenburg, Germany

PURPOSE. Mutations in the gene encoding Gasdermin A3 (*Gsdma3*) have been described to cause severe skin phenotypes, including loss of sebaceous glands and alopecia, in mice. We discovered a novel C-terminal mutation in *Gsdma3* in a new mouse line and characterized a less frequently reported corneal phenotype, likely caused by degeneration of Meibomian glands of the inner eyelid.

METHODS. We used histologic methods to evaluate the effects of the C+/H− mutation on sebaceous gland and skin morphology as well as Meibomian glands of the inner eyelid and corneal tissue. Chromosomal aberrations were excluded by karyogram analyses. The mutation was identified by Sanger sequencing of candidate genes.

RESULTS. Analyses of skin samples from affected mice confirmed the frequently reported phenotypes associated with mutations in *Gsdma3*: Degeneration of sebaceous glands and complete loss of pelage. Immunologic staining of corneal samples suggested an inflammatory response with signs of neovascularization in half of the affected older mice. While the corneal phenotype was observed at irregular time points, mainly after 6 months, its appearance coincided with a degeneration of Meibomian glands in the eyelids of affected animals.

CONCLUSIONS. The mutation described herein is associated with inflammation and neovascularization of corneal tissue. Simultaneous degeneration of Meibomian glands in affected animals suggested a change in tear-film composition as the underlying cause for the corneal phenotype. Our data further support that different pathogenic mechanisms underlie some of the reported mutations in *Gsdma3*.

Keywords: alopecia, meibomian gland, corneal inflammation, tears

Mutations in the C-terminal region of *Gsdma3*, the gene encoding the Gasdermin A3 protein in mice, lead to a phenotype characterized by complete hair-loss, hyperkeratinization of the skin, and degeneration of sebaceous glands in adult mice. Holocrine gland degeneration occasionally affects the Meibomian glands of the inner eyelid, leading to inflammation of the corneal epithelium and excessive proliferation of corneal tissue in older animals.[1–3]

Hair-loss is described in detail and is a phenotype observed in all 11 known *Gsdma3* mutant mouse lines (Alopecia [Ae],[4] Bareskin [Bsk],[5] Defolliculated [Dfl],[2] Finnegan [Fgn],[6] Michelin [M1Btlr], Mr. Magoo [M2Btlr], I359N [Mhdaclp1],[7] Reduced coat 2 [Rco2],[8] Rex-denuded [Re-Den],[9] recombination-induced mutation 3 [Rim3][1] and RIKEN00745/+[3]). Only a selection of publications described morphologic changes in the eyelid and cornea in detail.[1,2,8,10]

The phenotype of the corneal epithelium is likely a secondary effect of disrupted sebum secretion of defective Meibomian glands of the inner eyelid, leading to rapid evaporation of the tear-film that protects the cornea from drying-out.[2] Interestingly, Meibomian gland dysfunction is also associated with evaporative dry eye (EDE) disease, which is one of the most prevalent diseases of the human eye.[11–13]

The tear-film consists of a mucin, an aqueous and a lipid layer in varying ratios. Changes in its composition alter its protective and refractive properties.[13] Meibomian glands provide the outermost lipid layer of the tear-film, thereby preventing premature evaporation of tears and drying of the cornea.[14] This is achieved by secretion of lipid-filled lobular cells, which constantly regenerate from nearby progenitor cells.[15]

In the disease EDE, Meibomian glands show dysfunctional secretion of sebum. In the majority of cases, this is caused by an obstruction of their ductal system by cell debris or solidified sebum which, if untreated, can lead to further degeneration of the glands.[11,13] Phenotypically, EDE can manifest in an inflammation of corneal tissue or the eyelid itself and impairs the regeneration of corneal tissue after injury.[11] Treatment for the obstructive form of EDE consists of massages of the eyelid to loosen blockage of the Meibomian gland ducts and the application of artificial tears to rehydrate the eyes.[11] Since complete degeneration of Meibomian glands can be observed in untreated EDE cases, *Gsdma3* mutant mice that show a degeneration of Meibomian glands have the potential to serve as a disease model to understand the pathogenic processes of

the corneal alterations and the development of treatment options for the late stage of EDE.

Interestingly, the corneal phenotype is not described in all known *Gsdma3* mutants and for two of these mouse lines (Rco2 and RIKEN00745/+) even functional Meibomian glands have been observed, despite the absence of sebaceous glands in the skin of these animals.[3,8]

Gsdma3 is located on chromosome 11 in mice and encodes for the 464 amino acid protein Gasdermin A3, which is part of the Gasdermin family of proteins.[16] Saeki et al.[16] have found Gasdermin A3 to be primarily expressed in skin and stomach using Northern blot analysis, while Runkel et al.[8] detected *Gsdma3* mRNA in progenitor cells of Meibomian glands employing in situ hybridization. The protein is believed to play a role in the murine hair follicle cycle,[6,17,18] mammary gland development,[19] and mitochondrial homeostasis.[20] It displays a two-domain structure comprising a 35-kDa N-terminal and a 25-kDA C-terminal domain connected by an intermediate region.[21] While the majority of a total of 14 β-sheets are located in the N-terminal domain, most of the 12 α-helices are located in the globular C-terminal domain.[21]

In wild type, the C-terminal domain of Gasdermin A3 autoinhibits its N-terminal domain via interactions between helices α12 and α1, as well as helices α4, α9, and α11.[21] Upon cleavage of the protein at the intermediate region by an unknown activator, the C-terminal domain dissociates from the N-terminus, leading to its activation. All known *Gsdma3* mutations disrupt this autoinhibitory function of the C-terminus leading to constant activation of the N-terminal domain.[22] Activated N-terminal domains form pore-like multimers that incorporate into the cell membrane leading to pyroptotic cell death of lipid-filled gland cells.[21]

In this study, we describe a novel mutation (C+/H–: cornea plus, hair minus) in the far C-terminal region of Gasdermin A3 that causes both skin and corneal phenotypes. This mouse model develops its corneal phenotype likely due to Meibomian gland deficiency and might serve as a disease model for late stage EDE.

MATERIALS AND METHODS

Mice

The novel mutation described herein arose spontaneously in a BL6/J line that carries a homozygous mutation in the gene encoding membrane-type frizzled-related protein (MFRP$^{rd6/rd6}$). Affected mice were discovered by their obvious hairless appearance and backcrossed to MFRP$^{wt/wt}$ BL6/J.

Mice were anesthetized and killed by cervical dislocation at different time points (postnatal days 7 and 28 [P7 & P28], 2 months [M], 3M, 4M, 6M, and older) to prepare skin and cornea, as well as eyelid samples for further analysis.

All animal experiments adhere to the ARVO Statement for the Use of Animals in Ophthalmic and Vision Research and were approved by the Niedersächsisches Landesamt für Verbraucherschutz und Lebensmittelsicherheit (LAVES, reference number 14-1671).

Analysis of Skin and Cornea Morphology

Skin samples were prepared from five different body regions: cranial, dorsal-cranial, dorsal, ventral, and axillary and fixed in Roti Histofix 4% (Carl Roth, Karlsruhe, Germany) for several days. The fixed tissue was embedded in paraffin (Carl Roth) and cut to 4- to 7-μm slices on a Jung HN40 sliding microtome (Leica Biosystems, Nussloch, Germany). Whole eyes were prepared in the same manner for analysis of corneal morphology. Upper eyelids from affected animals and wild type littermates were fixed for 2 hours in 4% paraformaldehyde (Carl Roth), embedded in TissueTek OCT compound 4583 (Sakura Finetek GmbH, Staufen, Germany), and cut to 20-μm slices on a Leica CM1860 cryotome (Leica, Wetzlar, Germany).

Histologic staining of skin and cornea samples was performed using the hematoxylin-eosin (HE) method. Slices were deparaffinized by incubation in xylol (3 minutes; Carl Roth) followed by ethanol (100%, 95%, 70%, 1 minute each; Carl Roth) and stained with Mayers hematoxylin (1 minute; Fa. Walter, Kiel, Germany) and eosin (2.5 minutes; Merck, Darmstadt, Germany) solutions. For dehydration, slices were incubated in 70% ethanol for 70 seconds followed by 95%, 100% ethanol and xylol for 100 seconds each and embedded in Roti Histokitt II medium (Carl Roth). All steps were performed at room temperature (RT).

Eyelids were stained with HE according to the following protocol: 2-minute wash with ddH$_2$O, 30-second staining with Mayers hematoxylin (Carl Roth), 15-minute rinse with tap water, 30-second counter staining with eosin G solution (Carl Roth), and dehydration with 70%, 95%, and 100% ethanol and xylol (2 minutes each). After dehydration, slices were embedded in Roti Histokitt II medium (Carl Roth). All steps were performed at RT.

Sudan III staining was performed by 2-minute wash with ddH$_2$O, 10-minute incubation in Sudan III solution (3% Sudan III dissolved in 10% ethanol/90% acidic acid; Carl Roth), 2-minute differentiation in 50% ethanol, and a final 2-minute wash with ddH$_2$O at RT.

Slices were embedded in Roti Histokitt II medium (Carl Roth) and scanned on a Zeiss Axio Scope A1 (Carl Zeiss, Jena, Germany) at magnifications of 50× and 200× using Zeiss ZEN Software version 2.3.

Antibody staining of corneas and eyelids was carried out employing the following protocol: 3 times 5-minute wash with 0.1 M phosphate buffer (PB; pH 7.4; Carl Roth), 60-minute incubation in blocking solution at RT (0.1 M PB with 3% bovine serum albumin and 0.5% Triton X-100; Carl Roth), incubation with primary antibody over night at 4°C, 3 times 5-minute wash with PB at RT, 120-minute incubation with secondary antibody (in blocking solution), and three final washing steps with PB (5 minutes each) at RT. Slices were embedded in Dako Fluorescent Mounting Medium (Carl Roth) and scanned on a Leica DMRE confocal microscope with a TCS laser unit (Leica) using Zeiss 40× and 63× oil-immersion objectives (Carl Zeiss). Images were processed with FIJI version 1.49 (http://fiji.sc, in the public domain).

The following antibodies were used: rabbit anti-Laminin (Novus Biological, Abington, UK; NB300-144, 1:500), rat anti-mCD3 (R&D Systems, Minneapolis, MN, USA; MAB4841, clone 17A2, 1:500), donkey anti-rabbit Alexa 488 conjugated (Life Technologies, Carlsbad, CA, USA; 1:1000), donkey anti-rabbit Alexa 647 conjugated (Life Technologies; 1:1000), and goat anti-rat Alexa 488 conjugated (Invitrogen, Carlsbad, CA, USA; 1:1000).

The number of mice analyzed in the different disease stages were: P7–P28 (onset of skin phenotype): $n = 11$; 2M–5M (development of skin phenotype): $n = 22$; 6M–10M (onset and development of corneal phenotype): $n = 14$; 11M–17M (late stages of corneal phenotype): $n = 29$.

Macroscopic Analysis of Corneal Tissue

Macroscopic imaging of mouse eyes was carried out on an Olympus SZ51 binocular with an Olympus KL300 LED light (Olympus Deutschland GmbH, Hamburg, Germany).

Metaphase Chromosomes Preparations

Chromosomes were obtained from lymphocyte cultures according to Arakaki and Sparkes[23] methods. The 1 mL Na-heparin stabilized peripheral blood was cultivated for 72 hours in the culture medium containing 10 mL RPMI-1640 (Sigma-Aldrich Corp., St. Gallen, Switzerland) with 1.5 mL FCS, mitogen Pokeweed 0.35 mL (Sigma-Aldrich Corp.), Amphotericin 0.1 mL (Sigma-Aldrich Corp.) and penicillin + streptavidin 0.1 mL (Roche, Basel, Switzerland). The lymphocytes were treated with Colcemid (0.5 mL for each 10 mL of culture medium) for 2 hours (KaryoMAX Colcemid Solution in PBS; Gibco, Darmstadt, Germany, category number: 15212012, concentration 10 µg/mL). After centrifugation (800 rpm, 8 minutes, +24°C) and removal of the supernatant, a hypotonic KCl solution (0.075 M, +37°C) was added drop-wise up to 12 mL. Then cells were incubated for 20 to 25 minutes at +37°C. After this incubation, further centrifugation and removal of supernatant, cells were fixated by slowly dropping the frozen (−30°C) Carnoy's fixative (absolute methanol and glacial acetic acid in proportion 3:1) up to 15 mL. The samples were centrifuged (800 rpm, 8 minutes, +4°C) and the supernatant was discarded. The Carnoy's fixative was newly added up to 10 mL.

The concentrated chromosome suspension was finally dropped onto cold, humid microscope slides (10 µL per slide) and incubated at +37°C for 24 hours.

Multicolor Fluorescence In Situ Hybridization (mFISH)

mFISH was performed according to the MetaSystem protocol for Mouse Multicolor FISH Probes (MetaSystems Probes GmbH, Altlussheim, Germany, category number D-0425-120-DI). An Axio Imager Z1 microscope (Carl Zeiss AG, Feldbach, Switzerland) with a fluorescent 100-watt mercury lamp (HBO), filter set and ISIS imaging system for mFISH was used for microscopic analyses. In total, 50 metaphases were captured and analyzed. For each animal, three karyograms were performed.

DNA Extraction and PCR Amplification of *Gsdma3*

DNA was extracted from tail biopsies taken at P14. Tail biopsies were incubated in 600 µL TNES2 buffer (100 mM Tris pH 8.0, 200 mM NaCl, 5 mM EDTA, 0.2% SDS [Carl Roth] and 100 mg/mL Proteinase K [New England Biolabs, Frankfurt a.M., Germany]) at 55°C overnight while shaking at 1000 rpm. Lysed tail biopsies were centrifuged at 10,000g for 5 minutes the next day. Supernatant was diluted 1:100 with ddH$_2$O and used for PCR amplification of *Gsdma3* and Sanger sequencing. Amplification of *Gsdma3* exons and flanking intronic regions was carried out using intronic primers (see Supplementary Data) with the following PCR protocol on a Bio-Rad T100 Thermal Cycler (Bio-Rad Laboratories GmbH, Munich, Germany): initial denaturation: 15:00 at 95°C; (denaturation: 0:45 at 95°C, annealing: 0:45 at 60°C, elongation: 0:30 at 72°C) ×35; final elongation: 10:00 at 72°C; hold at 10°C.

Sanger Sequencing of *Gsdma3* Gene

All 11 exons and flanking intronic regions of *Gsdma3* were sequenced using intronic primers (see Supplementary Data). Sequencing was performed on ABI Prism 3130xl Genetic Analyzer (Applied Biosystems, Carlsbad, CA, USA) according to Sanger's protocol[24] using BigDye Terminator version 3.1 (ThermoFisher Scientific, Darmstadt, Germany) and the following cycle-sequencing protocol: initial denaturation: 1:00 at 96°C; (denaturation: 0:10 at 96°C, annealing: 0:05 at 50°C, elongation: 1:15 at 60°C) ×15; (denaturation: 0:10 at 96°C, annealing: 0:05 at 50°C, elongation: 1:30 at 60°C) ×5; (denaturation: 0:10 at 96°C, annealing: 0:05 at 50°C, elongation: 2:00 at 60°C) ×10; hold at 10°C.

Based on the phenotype and genotype results, the pedigree of the first four generations of the C+/H− mouse line was generated (CeGaT Online tool, in the public domain, http://www.cegat.de/fuer-aerzte/stammbaumerstellung).

3D Modeling of Gasdermin A3 and SIFT Prediction

A 3D model of *Gsdma3*[21] was obtained from the Protein Data Bank in Europe (in the public domain, https://www.ebi.ac.uk/pdbe/entry/pdb/5B5R) and modified using JMol version 14.10.0 (in the public domain, http://jmol.sourceforge.net/).

Impact of amino acid changes in the primary structure of Gasdermin A3 was evaluated using SIFT scoring[25] at http://sift.jcvi.org (in the public domain), using the amino acid sequence of wild-type Gasdermin A3 as reference.

RESULTS

The C+/H− Mouse Is Affected by a *Gsdma3* Mutation Showing an Autosomal-Dominant Mode of Inheritance

Analysis of a four-generation pedigree (Fig. 1A) suggested an autosomal-dominant mode of inheritance as both sexes were equally affected and the percentage of affected offspring was approximately 50% in every generation.

The karyograms of affected animals showed no obvious differences to unaffected littermates (Fig. 1B). We found no indication of chromosomal aberrations, neither balanced or unbalanced. Furthermore, trisomic karyograms were not detected. This suggested that chromosomal aberrations are not the cause of the dominant inheritance leading to the C+/H− phenotype.

The phenotypic similarities between C+/H− and previously described mouse models suggested *Gsdma3* as a candidate gene. Sanger sequencing of the coding exons and flanking intronic regions revealed a 1-bp insertion in exon 11 of *Gsdma3* (c.1280_1281insC, Fig. 1C) resulting in a frame shift (p.Gln427Pro*fs**30) in the amino acid sequence and a premature stop codon at position 457.

C+/H− Mice Displayed Progressive Hair-Loss and Degeneration of Sebaceous Glands in the Skin

Affected animals were distinguishable from wild-type littermates by the appearance of skin folds at the neck at approximately P7 and an irregular first coat. Hair-loss started at approximately P21 at the snout and progressed caudally (see Supplementary Data, Figs. S1A, S1B).

A thinner second coat emerged at approximately P33 starting at the head of the animal that continued to grow toward the tail of the animal. Shortly after its appearance, the second coat was lost. Loss of the second coat showed a head-to-tail progression similar as observed with the first coat. Except eyelashes and vibrissae, the animals appeared furless at approximately 3 to 4 months of age (see Supplementary Data, Figs. S1C–S1F).

Morphologically, the skin of affected animals showed thickening of the epidermal layer as early as P7 (Figs. 2A, 2B) and progressive degeneration of sebaceous glands started at approximately P28 (Figs. 2C, 2D). Hair-follicles were still present at P28 and 2 months (Figs. 2E, 2F). At approximately 3 to 4 months of age, hair-follicles and sebaceous glands were absent from the skin of affected animals (Figs. 2G–J).
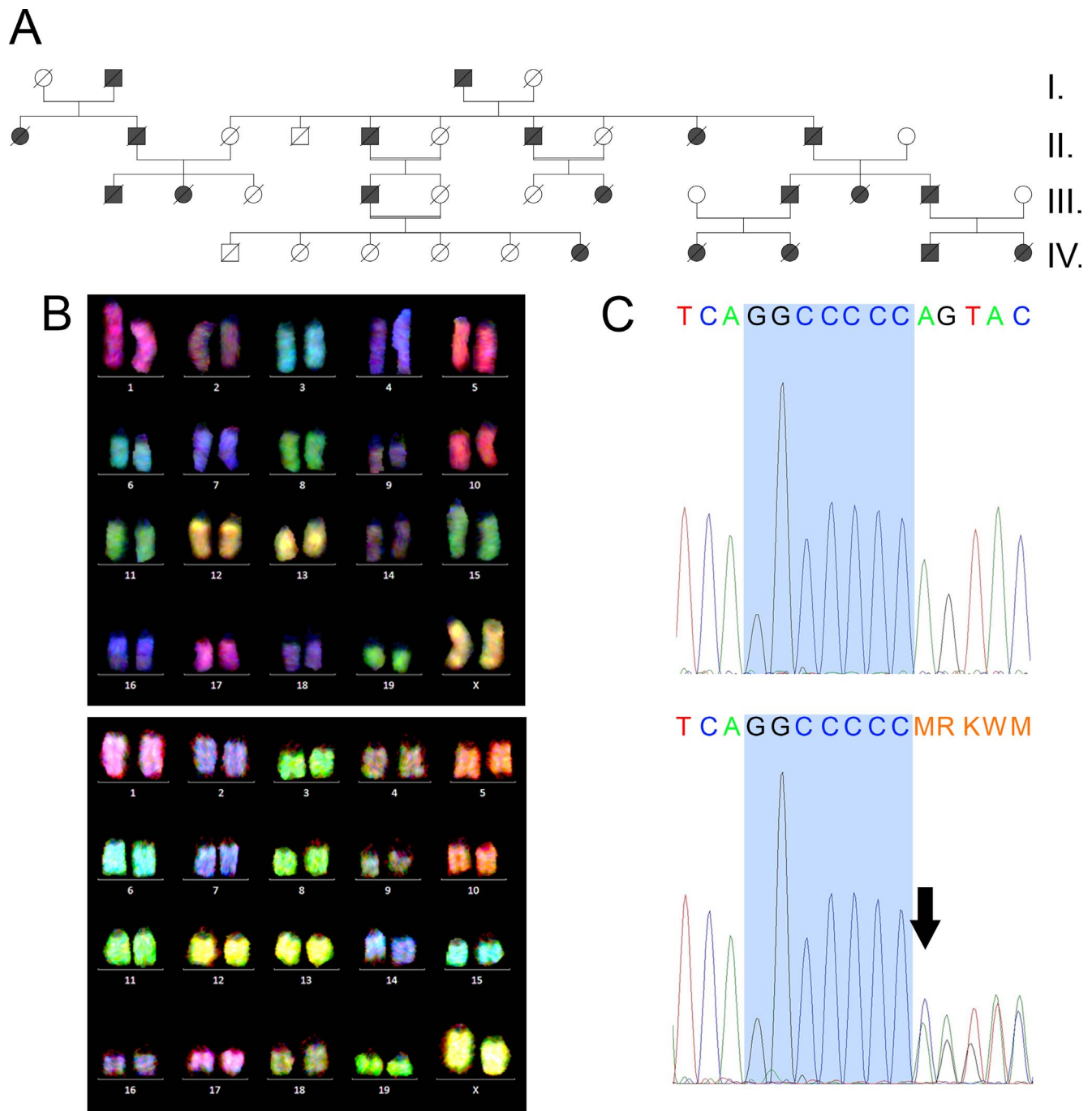
FIGURE 1. Genetic analyses of the C+/H− genotype. (**A**) The pedigree of the first four generations of the C+/H− mouse line revealed a homogenous distribution of affected and unaffected animals across both sexes and showed affected mice in every generation, highly suggestive of an autosomal dominant inheritance pattern. (**B**) Karyograms of an unaffected mouse (*upper panel*) and its affected littermate (*lower panel*) showed no obvious numerical or structural aberrations of the chromosomes. (**C**) Sanger sequencing of the candidate gene *Gsdma3* (*upper panel*: wild type sequence; *lower panel*: heterozygously mutated sequence) revealed an insertion of a single cystine base (*arrow*) in exon 11 of *Gsdma3* (c.1280_1281insC), which was predicted to lead to an amino acid exchange and a frame shift starting at Glutamine 427. The frame shift was predicted to result in a premature stop codon at position 457 (p.Gln427Pro*fs*30*).

Macroscopically, the skin of affected animals appeared brittle with a grayish color.

Half of C+/H− Mice Developed Corneal Opacities and Showed Inflammation of Corneal Tissue

Approximately half of C+/H− animals older than 6 months showed corneal opacities (Fig. 3A) that developed into a macroscopic increase of corneal tissue over time (Fig. 3B). In addition to these macroscopic alterations of the cornea, blood vessels seemed to have infiltrated the tissue and closure of the eyelid was impaired (Figs. 3C, 3D).

Out of a total of 186 heterozygotes, 104 animals (55.9%) developed a corneal phenotype with 38 animals unilaterally (20.4%) and 66 animals bilaterally (35.5%) affected. Only 10
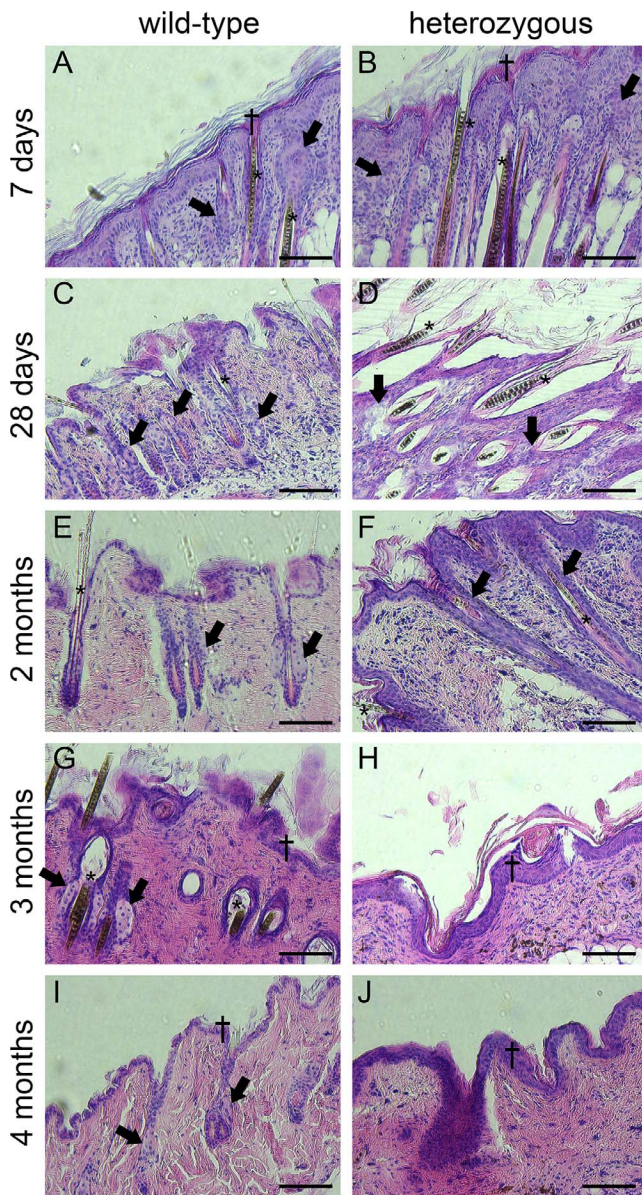
FIGURE 2. Microscopic appearance of the skin phenotype in C+/H− and wild-type mice. A slightly thickened epidermis (*crosses*) could be observed as early as P7 in C+/H− mice (**B**) compared to unaffected littermates (**A**). Sebaceous glands (*arrows*) started to degenerate at approximately P28 (**D**), while unaffected animals showed fully functional sebaceous glands during the entire observed time frame (**C**, **E**, **G**, **I**). Sebaceous glands were almost completely lost at 2 months of age (**F**) and absent from 3 months onwards (**H**, **J**) in C+/H− mice. Hair follicles were still present in the skin of affected mice until 2 months of age (**B**, **D**, **F**, *asterisks*) but were completely lost at 3 months (**H**, **J**). *Scale bars*: 50 μm.
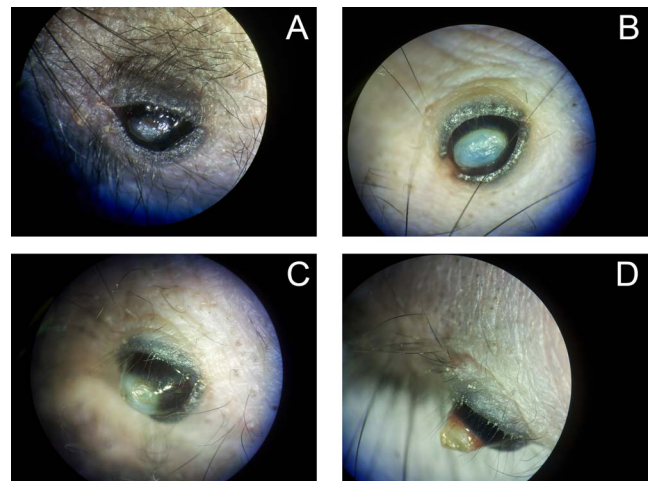

FIGURE 3. Macroscopic appearance of the corneal phenotype in older mice. Corneal opacities were observed starting at approximately 6 months of age in half of all affected mice. The corneal tissue did not show a macroscopic increase at this stage and the surface of the cornea appeared to remain smooth. (**A**, 7 months) Starting at the center of the cornea, an increase of tissue began forming a few weeks afterwards. This increase of cloudy tissue expanded both in width and depth (**B**, 8 months) and was infiltrated by blood vessels (**C**, 10 months). Tissue increase appeared to continue over the entire life span of the animals until eyelid closure was severely impaired (**D**, 12 months).

wild-type littermates showed normal morphology (Figs. 5A, 5B, 5E, 5F, 5I, 5J).

Antibody staining with anti-Laminin suggested angiogenesis of blood vessels in the stromal layer of the cornea (Figs. 6K, 6L, 6W, 6X, 6AA, 6AB). These vessels seemed to grow toward the epithelial layer (Figs. 6AA, 6AB, asterisks) and were morphologically observed in this layer at later stages (Fig. 5, asterisks). The central part of the cornea showed the most pronounced macroscopic increase. Infiltrating CD3^{+} T-cells are also present in this area (Figs. 6J, 6V, 6Z). Furthermore, the Descemet's membrane of the cornea appears compromised in C+/H− mice as shown by irregular or weakened laminin signals in animals that exhibit a clear corneal phenotype (Fig. 6, arrows). Epithelial blood vessels were present in wild-type (Figs. 6A–D, 6M–P, arrowheads) and unaffected C+/H− mice (Figs. 6E–H, 6Q–T, arrowheads) but undetectable in the epithelium of mice displaying a clear corneal phenotype (Figs. 6I–L, 6U–AB, arrowheads).

In older affected mice, the epithelial layer was also thickened (Figs. 5G, 5H, 5K, 5L, double crosses) and presented possible blood (asterisks) and lymphatic vessels (pluses). The corneal increase appeared to continue growing in size throughout the lifespan of the animal (Figs. 5K, 5L).

Meibomian Glands Showed Signs of Degeneration in the Eyelids of Affected C+/H− Mice

Morphologic analyses of upper eyelids of C+/H− mice aged 3M to 9M (Figs. 7C–L) revealed degeneration of Meibomian glands characterized by the absence of lobular cells (Fig. 7, crosses) and the appearance of cysts (Fig. 7, asterisks). Eyelids of wild-type littermates from the same age group showed fully developed lobular cells and did not develop cysts (Fig. 7A).

Staining with Sudan III to detect lipid content of Meibomian glands suggested an absence of lipid-filled globular cells in eyelids of C+/H− mice as early as 3 months of age (Fig. 7D), as well as in older mice (Figs. 7F, 7H, 7J, 7L). Wild-type littermates displayed normal lipid content (Fig. 7B).
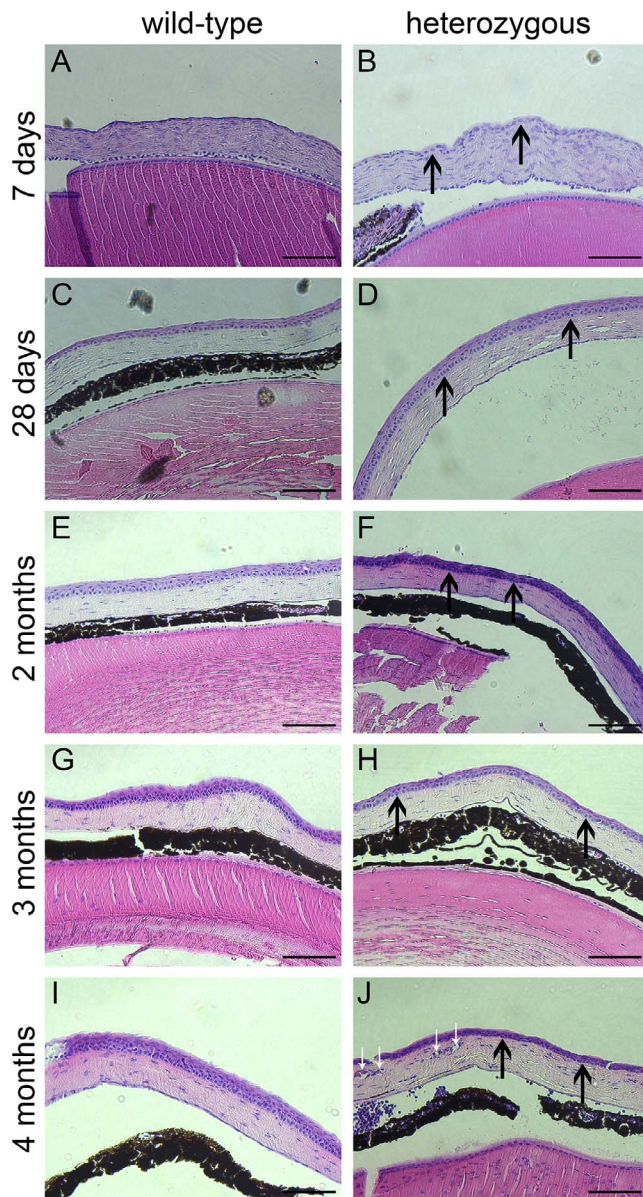
animals out of the 104 developed a corneal phenotype prior to the age of 6 months (9.6%).

In the first 3 months of life, histologic analysis of C+/H− corneas revealed no apparent morphologic differences between affected animals and their wild-type littermates (Figs. 4A–I). Neovascularization seemed to occur in corneas of some affected animals as early as 4 months of age (Fig. 4J).

An aberrant increase in size of the stromal layer (Figs. 5C, 5D, 5G, 5H, 5K, 5L) and possible signs of neovascularization (Fig. 5, asterisks) could be observed in approximately half of all C+/H− animals from 6 months onwards, while corneas of their

FIGURE 4. Microscopic appearance of the cornea in younger mice. During the first 3 months of life, corneal morphology of affected mice (**B, D, F, H**) showed no apparent differences to wild-type corneas (**A, C, E, G, I**). From 4 months onwards, corneas of affected mice seemed to show signs of neovascularization (**J**, *white arrows*). *Black arrows* point toward the basal epithelial layer. *Scale bars*: 50 μm.

The C+/H− Mutation Is Predicted to Cause Reorientation of Helix α12 and Disruption of Contacts Between Helices α12 and α1 in the Gasdermin A3 Protein

Insertion of one nucleotide in exon 11 of the *Gsdma3* gene (c.1280_1281insC, Fig. 8A) was predicted to cause a frame shift affecting the C-terminal 30 amino acids of the protein, thus leading to truncation of the last nine amino acids by a premature stop codon (Fig. 8B). Interestingly, this frame shift was predicted to lead to amino acid exchanges of aspartate 433 (p.Asp433Arg) and histidine 436 (p.His436Pro), two amino acids (Fig. 8B, open arrowheads) that have been described to directly interact with the N-terminal domain of Gasdermin A3.[21]

The frame shift is further predicted to incorporate eight helix-breaking prolines that likely prevent the formation of helix α12.

DISCUSSION

We describe a mouse model affected by a novel *Gsdma3* mutation that shows skin and sebaceous gland, as well as corneal and Meibomian gland phenotypes.

Gasdermin A3 is relevant to the process of pyroptotic cell death.[22,26] The C-terminal domain of Gasdermin A3 auto-inhibits its N-terminal domain.[26] Cleavage of the protein by its unknown activator leads to dissociation of the two domains, which activates the N-terminal portion of the protein. Activated N-termini migrate to the cell membrane and form pore-like multimers of 16 subunits that incorporate into the membrane and allow for discharge of cellular contents, resulting in pyroptotic cell death.[26] In wild type, a similar mechanism is observed in sebaceous glands of the skin and in the Meibomian glands of the eyelids where sebocytes undergo controlled cell-death, releasing their contents as sebum, which is secreted by these two glands.[27,28] In this context, Runkel et al.[8] has also speculated on a possible role of *Gsdma3* in the differentiation of progenitor cells into sebocytes. While the molecular process underlying controlled sebocyte death is different from pyroptosis[29] and possibly independent from Gasdermin A3, a dysfunction in Gasdermin A3 autoinhibition would lead to a premature discharge of cellular contents from basal cells of Meibomian glands, which later differentiate into sebocytes.[8]

C+/H− mice display both degeneration of the sebaceous glands in the skin and abnormal morphology of Meibomian glands, including loss of sebum-filled lobular cells and the appearance of large cysts in the eyelids.

Absence of lobular cells prevents the secretion of sebum from these glands onto the eye. This leads to a change in the composition of the tear-film, depriving it of lipid components[13,14] and influencing both its evaporation (which is fastened) and refractive index. Rapid evaporation of the protective tear-film then leads to dehydration of the cornea and severely reduced resistance to mechanical irritation, as well as bacterial or viral infection.[13,30] The reduction or loss of the protective tear-film likely is the cause for the corneal aberrations described in this report and in several other *Gsdma3* mutant mouse lines.[1,2,8]

Eyelids of affected C+/H− mice display degenerated Meibomian glands with reduced lipid content as early as age 3 months, the earliest time point at which a corneal phenotype could be observed in these mice. This suggests a correlation between Meibomian gland degeneration and the observed inflammatory reaction of the cornea. To further evaluate the link between these two phenotypes, a detailed examination of the molecular mechanisms in the eyelids of C+/H− animals is required at different time points.

Interestingly, dysfunction of Meibomian glands and the resulting changes in tear-film composition are also a prominent feature of EDE, one of the most prevalent diseases of the human eye.[13] While, in most cases, EDE is initially caused by an obstruction of Meibomian gland ducts by foreign material or tissue, a cystic degeneration of the Meibomian glands can be observed in later stages of untreated EDE.[11,31] Similarly, we and others observed cystic degeneration in the eyelids of C+/H− and other *Gsdma3* mutant mice.[3]

Similar as observed in late stage EDE patients, C+/H− mice display an inflammatory response of the cornea along with signs of neovascularization and possible angiogenesis.[32-36] This mouse model might serve as a useful animal model for EDE and
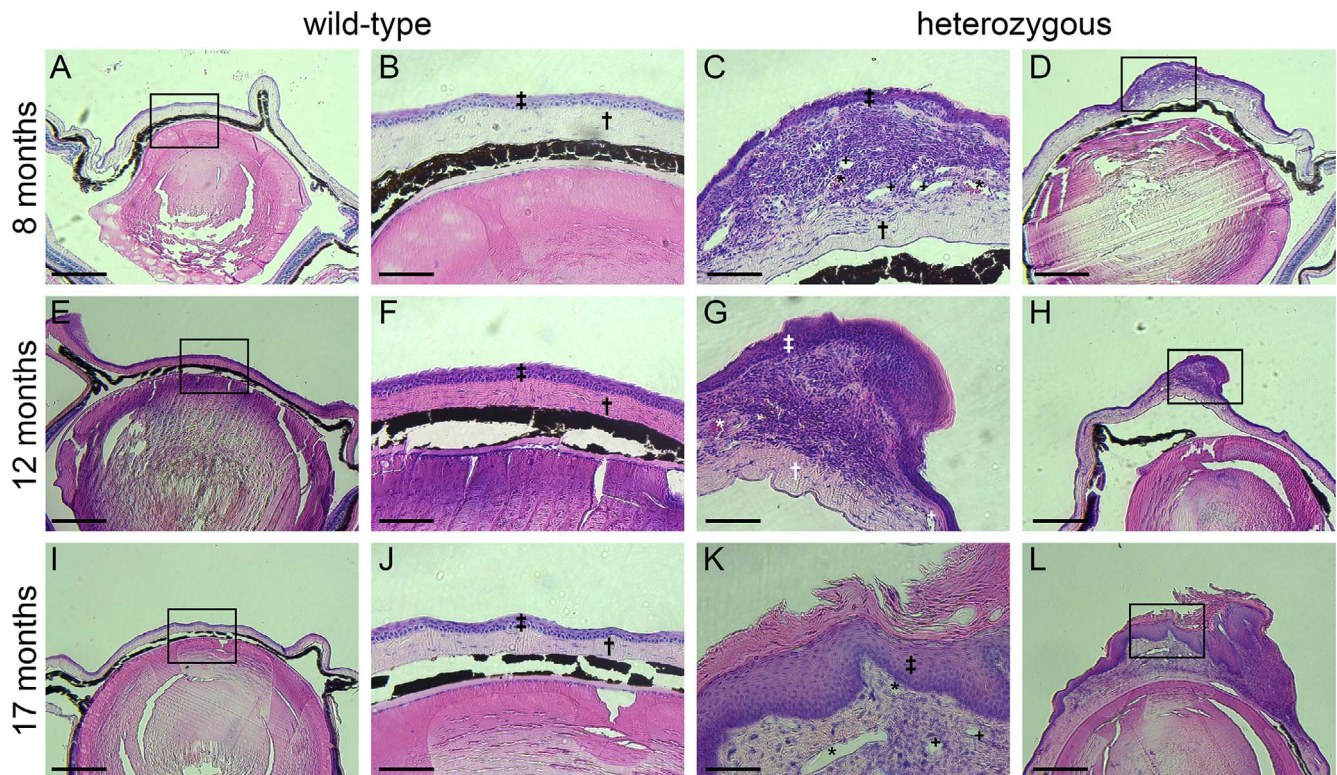
FIGURE 5. Morphologic changes of the cornea in C+/H− mice. Thickening of the stromal layer (*crosses*) of the cornea was observed at approximately 6 months of age in half of the affected mice, accompanied by increasing signs of neovascularization (**C**, **G**, **K**, *pluses*). Some of these newly formed vessels can be identified as blood vessels by the presence of clotted blood cells (**C**, **G**, **K**, *asterisks*). From 12 months onwards, the epithelial layer (*double crosses*) began to thicken and became disorganized (**G**, **K**). In very old mice (17 months, **K**, **L**) formation of an extra layer above the epithelium was observed, possibly consisting of dead epithelial cells. In comparison, corneas of unaffected littermates showed a normal, wild type morphology even at very old ages (**A**, **B**, **E**, **F**, **I**, **J**). *Scale bars*: 200 μm in overviews and 50 μm in magnifications.

would allow us to study the molecular and morphologic causes as well as the progression of Meibomian gland degeneration in vivo. A more in-depth description of the corneal phenotype including immunohistochemical and gene expression analyses of known molecular factors in corneal inflammation and neovascularization[36–41] (for review see Ref. 42) might help to establish the pathway of inflammatory response and vasculogenesis in these mice. This report provides an initial description of this new mouse line and hints at its possible use in EDE research.

The C+/H− mouse line further allows us to study the correlation between structural elements of the Gasdermin A3 protein and the phenotypes observed in *Gsdma3* mutant mice: on the molecular level, mutations in the C-terminal region of Gasdermin A3 were described to prevent efficient autoinhibition and lead to unregulated pyroptosis in cells expressing Gasdermin A3[22,26] including basal cells of the Meibomian glands.[8] In mice, this manifests phenotypically in complete hair-loss within the first 3 months of life due to degeneration of sebaceous glands in the skin of affected animals and the subsequent disruption of the natural haircycle.[18]

While the hair-loss phenotype can be observed in all known *Gsdma3* mutations, including C+/H−, the corneal phenotype is not consistently reported in these animals. The late onset of the corneal phenotype and its irregular occurrence support the hypothesis that it is a secondary effect caused by the degeneration of Meibomian glands. For a primary effect of the mutation, we would expect this phenotype to occur bilaterally in all animals carrying the mutation. Additionally, two *Gsdma3* mouse lines with functional Meibomian glands have been

observed (Rco2[8] and RIKEN00745/+[3]) and lack the corneal phenotype.

However, a clear correlation between the predicted severity of a mutation and presence of functional Meibomian glands in affected animals seems difficult. Based on SIFT scoring (in the public domain, http://sift.jcvi.org/), an online tool to predict the severity of mutations, two *Gsdma3* mutations, Rco2 (p.Leu343Pro) and RIKEN00745/+ (p.Tyr442*), incorporate amino acid changes that are predicted to severely influence protein structure and function (with a SIFT score of 0.00) but show intact Meibomian glands in combination with a severe skin phenotype.[3,8] While the RIKEN00745/+ p.Tyr442* mutation[3] only affects the last few amino acids of the C-terminus, the Rco2 p.Leu343Pro mutation[8] is located in a highly conserved stretch of amino acids in helix α8 where any kind of change is predicted to disrupt protein structure according to SIFT scoring. The exchange of leucine to proline should effectively break helix α8 in this mutation. Despite these putatively disruptive changes, Meibomian glands remain functional in Rco2 (age: 2 months[8]) and RIKEN00745/+ (age: 10 months[3]) mice while sebaceous glands are absent from the skin of these animals. In contrast, three other *Gsdma3* mutations (Ae, Bsk, and M2Btlr) show changes in the adjacent tyrosine residue (Ae: p.Tyr344His,[4] Bsk,[5] and M2Btlr: p.Tyr344Cys). These amino acid changes are predicted to only mildly influence protein structure (SIFT scores are 0.13 and 0.18, respectively), yet these mice show a corneal phenotype. Meibomian gland morphology was not described for these three mouse lines. However, tyrosine 344 is predicted to directly contact amino acids located in the N-terminal domain of Gasdermin A3,[21] which could explain the high impact of
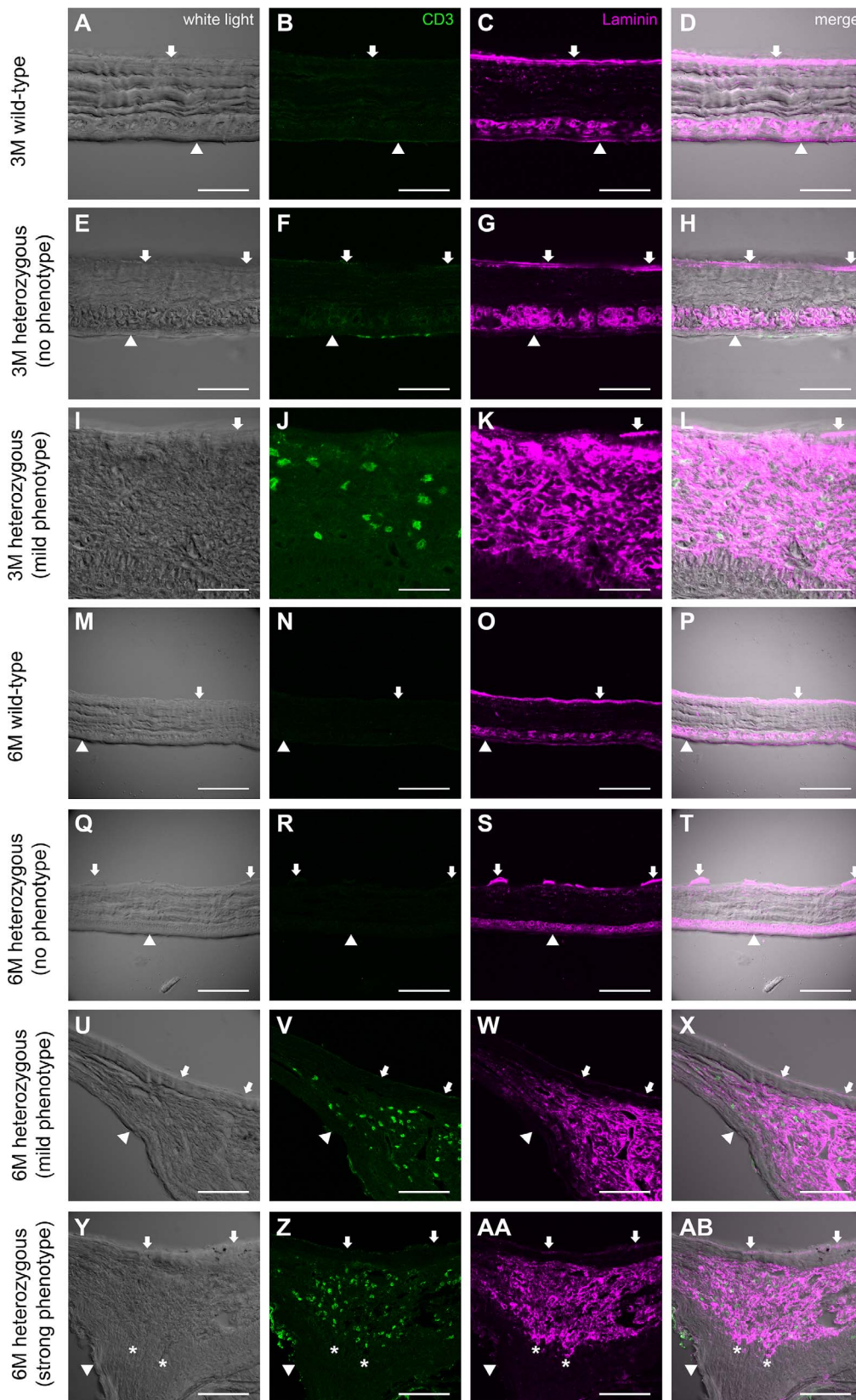
FIGURE 6. Immunohistochemical analyses of affected and unaffected corneas of 3M- and 6M-old mice. Corneas of wild type (**A–D, M–P**) and heterozygous C+/H− mice that do not display a macroscopic corneal phenotype (**E–H, Q–T**) showed normal morphology with laminin-positive (magenta) blood vessels present only in the epithelial layer (*arrowheads*) and a distinct, double layered Descemet's membrane stained by anti-laminin (*arrows*). In unaffected heterozygous C+/H− animals, the laminin staining showed a fragmented immunoreactivity pattern at the Descemet's membrane (**G, S,** *arrows*). No CD3+ T-cells (*green*) were detected in the corneas of these animals (**B, F, N, R**). C+/H− mice that displayed a macroscopic corneal phenotype (**I–L, U–AB**) showed weaker staining of the Descemet's membrane with anti-laminin (**K, W, AA,** *arrows*). Blood vessels appeared to be missing in the epithelium (**W, AA,** *arrowheads*). Putative blood and lymphatic vessels are present in the corneal stroma of these mice, possibly growing toward the epithelium (**AA, AB,** *asterisks*). *Scale bars*: 50 μm.

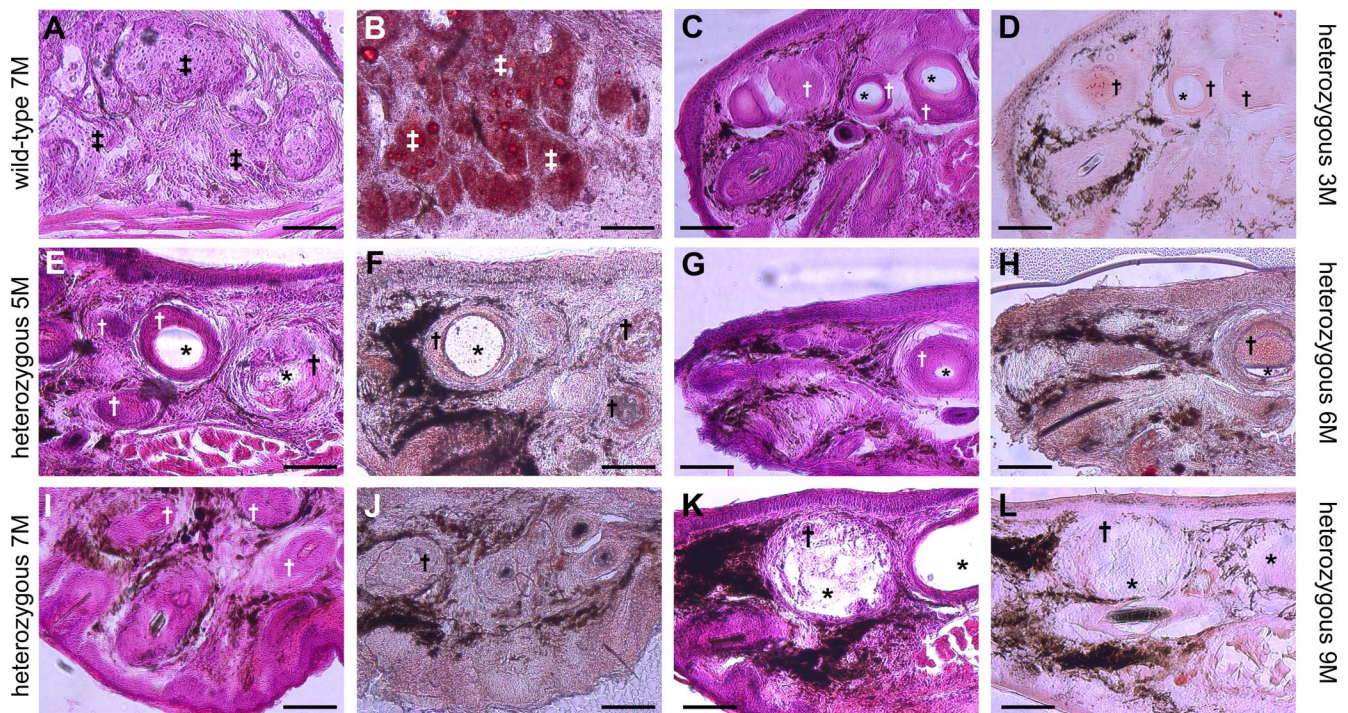Investigative Ophthalmology & Visual Science

FIGURE 7. Morphology and lipid-stain in upper eyelids of C+/H− mice and controls. Upper eyelids of wild-type mice displayed distinct populations of differentiated lobular cells that stain positive for lipid content (**A**, **B**, *double crosses*, *dark red signals* in **B**: Sudan III staining). Abnormal cysts were not observed in wild-type mice (**A**, **B**). Affected littermates (**C–L**) from the same age group displayed aggregates of degenerated lobular cells (*crosses*) that did not or weakly stain positive for lipids (*dark red signals* in **D**, **F**, **H**, **J**, **L**: Sudan III staining). Cysts of up to 50 μm in diameter were only detected in the eyelids of affected animals (*asterisks*). Consecutive slices were used for HE and Sudan III staining. *Scale bars*: 50 μm.

mutations in this particular residue compared to the milder phenotype observed in leucine 343 mutants.

The mutation described in this publication (p.Gln427Pro*fs**30) is located in the far C-terminal region of the protein, in a β-sheet structure preceding a turn directly upstream of the last helix (α12) of the Gasdermin A3 protein (Fig. 8A). The exchange of the wild type glutamine for proline at amino acid position 427 is expected to influence protein structure with a SIFT score of 0.01, possibly leading to a spatial reorientation of helix α12.

Furthermore, in the wild type protein, two amino acids located in helix α12 (Asp433 and His436) engage in direct contact with the very N-terminal helix α1 (contacting Arg13 and Asp6, respectively). These amino acids are changed to Arg433 and Pro436 in C+/H− mice (Fig. 8B, open arrowheads) and possibly display an altered spatial orientation due to the appearance of a proline residue at upstream position 427. This could potentially disrupt contact between helices α12 and α1.

The wild-type helix α12 is positioned centrally in a barrel-like structure formed by helices α5&6 and α9&10, which is flanked by helices α8 and α11 (Fig. 8A). The finding that the frame shift C+/H− mutation likely disrupts this structural element suggested that α12s central position in the barrel might be important for the integrity of the C-terminal domain. Mutations in helix α12 could therefore indirectly affect the positions of amino acids Ile359, Leu409, and Ala412 located in the two helices α9 and α11, possibly disrupting their ability to contact their N-terminal partners in helix α4.[21]

Additionally, the C+/H− mutation described herein causes a frame shift that severely alters the amino acid composition of the C-terminus and truncates the protein by nine amino acids. Due to the appearance of eight helix-breaking proline residues in the mutated C-terminus (Fig. 8B, asterisks), it is highly

unlikely that this region will form a helix and can sustain the wild-type structure of the C-terminal domain.

RIKEN00745/+ (p.Tyr442*) is the only other known *Gsdma3* mutation located in or near helix α12.[3] Interestingly, this mutation is neither described to result in a corneal phenotype nor in a degeneration of Meibomian glands.[3] This could suggest that truncation of helix α12 (as observed in RIKEN00745/+) impacts protein structure and function less severely than its spatial relocation or disruption of its helical structure (as predicted for the C+/H− mutation). Furthermore, the RIKEN00745/+ mutation does not affect Asp433 and His436, hence contact between helices α12 and α1 should still be possible. We speculate that this might be the reason for the missing corneal and Meibomian phenotypes in this mouse model.

It remains unclear whether positioning and secondary structure of helix α12 have any impact on protein function or if the severe phenotype of C+/H− mice solely stems from the disrupted contact between helices α12 and α1 due to the amino acid changes at positions 433 and 436.

While the appearance of functional Meibomian glands in Rco2 and RIKEN00745/+ suggests that the integrity of these contact points is paramount for Meibomian gland function, it will be a matter of further experiments to test this hypothesis. It is highly interesting that mutations in different regions of the Gasdermin A3 protein (and even mutations in two adjacent amino acid residues) can lead to such opposing Meibomian gland phenotypes.

To summarize, we described a novel mouse line, C+/H−, carrying a C-terminal mutation in *Gsdma3*, which displays skin and corneal phenotypes. Due to a degeneration of Meibomian glands, this mouse line could serve as an animal model for late stage EDE, one of the most prevalent diseases of the human eye.
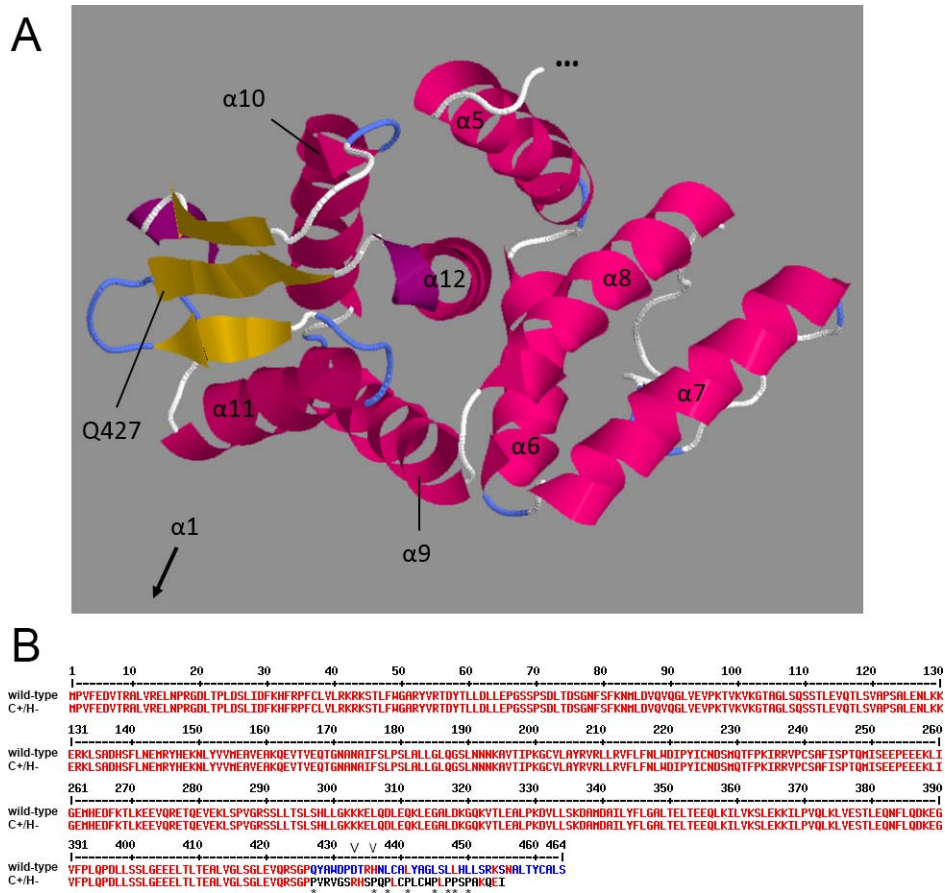
FIGURE 8. Protein structure and sequence of Gasdermin A3. 3D structure of the wild-type Gasdermin A3 C-terminal domain showing amino acids 264-464 (**A**). Helix α12 inserts centrally into a barrel-like structure formed by helices α5&6 and α9&10. The frame shift C+/H− mutation is located directly upstream of helix α12 in a short β-sheet structure preceding the final turn of the protein. Q427 marks the first amino acid changed by the frame shift. The approximate position of the most N-terminal helix α1 is annotated. The frame shift caused by the C+/H− mutation is predicted to lead to the appearance of eight helix-breaking proline residues (**B**, *asterisks*) in helix α12. Amino acids contacting N-terminal helix α1 in the wild-type protein (Asp433 and His436) are exchanged for arginine and proline in the mutated protein (*open arrowheads*).

References

1. Sato H, Koide T, Masuya H, et al. A new mutation Rim3 resembling Re(den) is mapped close to retinoic acid receptor alpha (Rara) gene on mouse chromosome 11. *Mamm Genome*. 1998;9:20–25.

2. Porter RM, Jahoda CA, Lunny DP, et al. Defolliculated (dfl): a dominant mouse mutation leading to poor sebaceous gland differentiation and total elimination of pelage follicles. *J Invest Dermatol*. 2002;119:32–37.

3. Tanaka S. *Functional Analysis of Rim3 Mutation That Exhibits Aberrant Epidermal Morphogenesis* [doctoral thesis]. The Graduate University for Advanced Studies; 2004.

4. Li J, Zhou Y, Yang T, Wang N, Lian X, Yang L. Gsdma3 is required for hair follicle differentiation in mice. *Biochem Biophys Res Commun*. 2010;403:18–23.

5. Lyon MF, Glenister PH. Mouse News Letter No. 71. *Mouse News Letter*. 1984; 71.

6. Lunny DP, Weed E, Nolan PM, Marquardt A, Augustin M, Porter RM. Mutations in gasdermin 3 cause aberrant differentiation of the hair follicle and sebaceous gland. *J Invest Dermatol*. 2005;124:615–621.

7. Kumar S, Rathkolb B, Budde BS, et al. Gsdma3(I359N) is a novel ENU-induced mutant mouse line for studying the function of Gasdermin A3 in the hair follicle and epidermis. *J Dermatol Sci*. 2012;67:190–192.

8. Runkel F, Marquardt A, Stoeger C, et al. The dominant alopecia phenotypes Bareskin, Rex-denuded, and Reduced Coat 2 are caused by mutations in gasdermin 3. *Genomics*. 2004;84:824–835.

9. Snell GD, Bunker HP. Mouse News Letter No. 39. *Mouse News Letter*. 1968; 39.

10. Shiraishi A, Kao CW, Ishizaki M, et al. Characterization of Bsk mice: I. The Bsk mutation does not involve a recombination of cornea-specific keratin 12 and skin-specific hair keratin genes. *Curr Eye Res*. 1998;17:531–540.

11. Knop E, Knop N, Brewitt H, et al. Meibomian glands: part III. Dysfunction - argument for a discrete disease entity and as an important cause of dry eye [in German]. *Ophthalmologe*. 2009;106:966–979.

12. Cuevas M, Gonzalez-Garcia MJ, Castellanos E, et al. Correlations among symptoms, signs, and clinical tests in evapora-

tive-type dry eye disease caused by Meibomian gland dysfunction (MGD). *Curr Eye Res*. 2012;37:855–863.

13. Rolando M, Zierhut M. The ocular surface and tear film and their dysfunction in dry eye disease. *Surv Ophthalmol*. 2001;45(suppl 2):S203–210.

14. Mishima S, Maurice DM. The oily layer of the tear film and evaporation from the corneal surface. *Exp Eye Res*. 1961;1:39–45.

15. Olami Y, Zajicek G, Cogan M, Gnessin H, Pe'er J. Turnover and migration of meibomian gland cells in rats' eyelids. *Ophthalmic Res*. 2001;33:170–175.

16. Saeki N, Kuwahara Y, Sasaki H, Satoh H, Shiroishi T. Gasdermin (Gsdm) localizing to mouse Chromosome 11 is predominantly expressed in upper gastrointestinal tract but significantly suppressed in human gastric cancer cells. *Mamm Genome*. 2000;11:718–724.

17. Lei M, Gao X, Yang L, Yang T, Lian X. Gsdma3 gene is needed for the induction of apoptosis-driven catagen during mouse hair follicle cycle. *Histochem Cell Biol*. 2011;136:335–343.

18. Tanaka S, Tamura M, Aoki A, et al. A new Gsdma3 mutation affecting anagen phase of first hair cycle. *Biochem Biophys Res Commun*. 2007;359:902–907.

19. Guo H, Xu S, Liu Y, et al. Gsdma3 is required for mammary gland development in mice. *Histochem Cell Biol*. 2017;147:575–583.

20. Lin PH, Lin HY, Kuo CC, Yang LT. N-terminal functional domain of Gasdermin A3 regulates mitochondrial homeostasis via mitochondrial targeting. *J Biomed Sci*. 2015;22:44.

21. Ding J, Wang K, Liu W, et al. Pore-forming activity and structural autoinhibition of the gasdermin family. *Nature*. 2016;535:111–116.

22. Shi P, Tang A, Xian L, et al. Loss of conserved Gsdma3 self-regulation causes autophagy and cell death. *Biochem J*. 2015;468:325–336.

23. Arakaki DT, Sparkes RS. Microtechnique for culturing leukocytes from whole blood. *Cytogenetics*. 1963;2:57–60.

24. Sanger F, Nicklen S, Coulson AR. DNA sequencing with chain-terminating inhibitors. *Proc Natl Acad Sci U S A*. 1977;74:5463–5467.

25. Ng PC. SIFT: predicting amino acid changes that affect protein function. *Nucleic Acids Res*. 2003;31:3812–3814.

26. Shi J, Zhao Y, Wang K, et al. Cleavage of GSDMD by inflammatory caspases determines pyroptotic cell death. *Nature*. 2015;526:660–665.

27. Niemann C. Differentiation of the sebaceous gland. *Dermatoendocrinol*. 2009;1:64–67.

28. Thiboutot D. Regulation of human sebaceous glands. *J Invest Dermatol*. 2004;123:1–12.

29. Schneider MR, Paus R. Sebocytes, multifaceted epithelial cells: lipid production and holocrine secretion. *Int J Biochem Cell Biol*. 2010;42:181–185.

30. Rolando M, Refojo MF, Kenyon KR. Tear water evaporation and eye surface diseases. *Ophthalmologica*. 1985;190:147–149.

31. Gutgesell VJ, Stern GA, Hood CI. Histopathology of meibomian gland dysfunction. *Am J Ophthalmol*. 1982;94:383–387.

32. El Annan J, Goyal S, Zhang Q, Freeman GJ, Sharpe AH, Dana R. Regulation of T-cell chemotaxis by programmed death-ligand 1 (PD-L1) in dry eye-associated corneal inflammation. *Invest Ophthalmol Vis Sci*. 2010;51:3418–3423.

33. Abdelfattah NS, Amgad M, Zayed AA. Host immune cellular reactions in corneal neovascularization. *Int J Ophthalmol*. 2016;9:625–633.

34. Cursiefen C, Maruyama K, Jackson DG, Streilein JW, Kruse FE. Time course of angiogenesis and lymphangiogenesis after brief corneal inflammation. *Cornea*. 2006;25:443–447.

35. Pearlman E, Sun Y, Roy S, et al. Host defense at the ocular surface. *Int Rev Immunol*. 2013;32:4–18.

36. Solomon A, Dursun D, Liu Z, Xie Y, Macri A, Pflugfelder SC. Pro- and anti-inflammatory forms of interleukin-1 in the tear fluid and conjunctiva of patients with dry-eye disease. *Invest Ophthalmol Vis Sci*. 2001;42:2283–2292.

37. Li D-Q, Tseng SCG. Three patterns of cytokine expression potentially involved in epithelial-fibroblast interactions of human ocular surface. *J Cell Phys*. 1995;163:61–79.

38. Narayanan S, Glasser A, Hu Y-S, McDermott AM. The effect of interleukin-1 on cytokine gene expression by human corneal epithelial cells. *Exp Eye Res*. 2005;80:175–183.

39. Kuriyan AE, Lehmann GM, Kulkarni AA, et al. Electrophilic PPARgamma ligands inhibit corneal fibroblast to myofibroblast differentiation in vitro: a potentially novel therapy for corneal scarring. *Exp Eye Res*. 2012;94:136–145.

40. Jeon KI, Kulkarni A, Woeller CF, et al. Inhibitory effects of PPARgamma ligands on TGF-beta1-induced corneal myofibroblast transformation. *Am J Pathol*. 2014;184:1429–1445.

41. Kvanta A, Sarman S, Fagerholm P, Seregard S, Steen B. Expression of matrix metalloproteinase-2 (MMP-2) and vascular endothelial growth factor (VEGF) in inflammation-associated corneal neovascularization. *Exp Eye Res*. 2000;70:419–428.

42. Ma DH, Chen JK, Zhang F, Lin KY, Yao JY, Yu JS. Regulation of corneal angiogenesis in limbal stem cell deficiency. *Prog Retin Eye Res*. 2006;25:563–590.

Investigative Ophthalmology & Visual Science